Photon Isolation and Jet Substructure

by

Zachary Hall

Submitted to the Department of Physics
in partial fulfillment of the requirements for the degree of

Bachelor of Science in Physics

at the

MASSACHUSETTS INSTITUTE OF TECHNOLOGY

June 2018

Signature redacted

Author .....
.....
Department of Physics
May 11, 2018

Signature redacted

Certified by.....
.....
Jesse Thaler
Associate Professor of Physics
Thesis Supervisor

Signature redacted

Accepted by ..
.....
Scott Hughes
Interim Physics Associate Head

Photon Isolation and Jet Substructure

by

Zachary Hall

Submitted to the Department of Physics
on May 11, 2018, in partial fulfillment of the
requirements for the degree of
Bachelor of Science in Physics

Abstract

We introduce soft drop isolation, a new photon isolation criterion inspired by jet substructure techniques. Soft drop isolation is collinear-safe and is equivalent to Frixione isolation at leading order in the small R limit. However, soft drop isolation has the interesting feature of being democratic, meaning that photons can be treated equivalently to hadrons for initial jet clustering. Taking advantage of this democratic property, we define an isolated photon subjet: a photon that is not isolated from its parent jet but is isolated within its parent subjet after soft drop declustering. The kinematics of this isolated photon subjet can be used to expose the QED splitting function, in which a quark radiates a photon, and we verify this behavior using both a parton shower generator and a perturbative calculation in the collinear limit.

Thesis Supervisor: Jesse Thaler
Title: Associate Professor of Physics

Acknowledgments

The material in this thesis is derived from work to be submitted for publication co-authored with Jesse Thaler [1]. I would like to thank Prof. Thaler for his invaluable mentorship and advice throughout the writing of this thesis. We thank Stefano Frixione and Mike Williams for interesting discussions. This work was in part supported by the MIT Undergraduate Research Opportunities Program.

Contents

List of Figures

Chapter 1

Introduction

Photons produced in high-energy collisions fall into two categories: "direct" photons produced in perturbative hard processes and "indirect" photons produced from the fragmentation of quark and gluon partons. Because direct photons access the perturbative part of the collision, they are of typically of more interest than indirect photons. For this reason, photon isolation techniques have been developed to filter out indirect photons [2–11]. Although there are different types of isolation criteria used, they all follow roughly the same philosophy: photons collinear to a significant amount of hadronic energy are labeled indirect, while photons well separated from hadronic energy are labeled direct. By now, photon isolation is a well-established method to study direct photons, with numerous measurements at the Large Hadron Collider (LHC) and previous experiments [6, 12–18].

In the years since the development of photon isolation, jet physics has undergone a rapid evolution, first with the rise of clustering-based jet observables [19–26] and more recently with the explosion of the field of jet substructure [27–36]. Jet substructure provides a rich toolbox to explore soft and collinear dynamics within jets, and it is natural to ask whether substructure techniques could be adapted to handle photons. At minimum, jet substructure could be used to robustly veto hadronic activity and isolate direct photons. More ambitiously, jet substructure could facilitate new methods to study indirect photons, by revealing a continuum of collinear photon fragmentation processes from perturbative radiation to hadronic decays.

In this paper, we introduce a new substructure-based photon isolation technique called *soft drop isolation*. This method derives from soft drop declustering [37], one of many jet grooming algorithms [31, 38–41] that have been successfully adopted at the LHC. Ordinarily, soft drop declustering is used to identify hard subjets within a jet that satisfy the condition:

$$\frac{\min\left(p_{T1}, p_{T2}\right)}{p_{T1} + p_{T2}} \geq z_{\text{cut}} \left(\frac{R_{12}}{R_0}\right)^{\beta}, \tag{1.1}$$

where p_{Ti} are the transverse momenta of the subjets, R_{12} is their pairwise angular separation, R_0 is the jet radius parameter, and z_{cut} and β are the parameters of the soft drop algorithm. Soft drop isolation *inverts* the condition in Eq. (1.1), thereby selecting "photon jets" with no appreciable substructure. With its origins in jet substructure, soft drop isolation is well suited to the age of particle flow at both CMS [42] and ATLAS [43].

Like Frixione isolation [10], soft drop isolation is collinear-safe and fully regulates the collinear divergence of quark-to-photon fragmentation. This is in contrast with cone isolation techniques [2–6], which are collinear-unsafe. In fact, soft drop isolation is equivalent at leading order to the most common implementation of Frixione isolation, at least when considering the small R_0 and small z_{cut} limits. Unlike Frixione isolation or cone isolation, though, soft drop isolation is democratic, meaning that it treats photons and hadrons equivalently in the initial clustering step. This feature is reminiscent of earlier democratic isolation criteria [7–9], which can be more natural than undemocratic criteria in cases where jets are the central objects of interest. Soft drop isolation is, to our knowledge, the first collinear-safe democratic photon isolation criterion.

In the second half of this paper, we take advantage of the democratic nature of soft drop isolation to define an isolated photon subjet: a photon that is not isolated from its parent jet but which is isolated within its parent subjet. At leading order in the collinear limit, isolated photon subjets arise from the splitting of a quark into a quark plus a photon in quantum electrodynamics (QED), as shown in Fig. 1-1a.

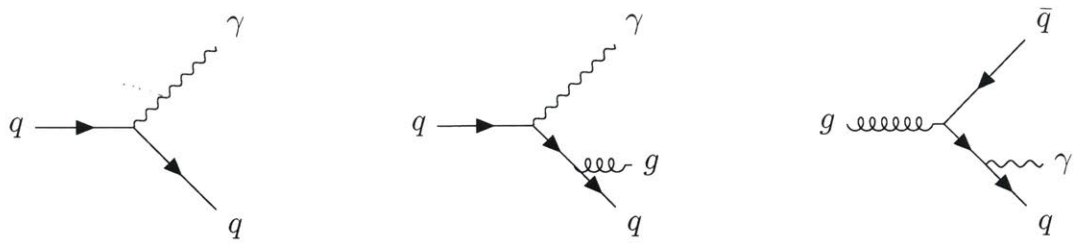

(a) (b) (c)

Figure 1-1: **(a)** Isolated photon subjet production from a quark at order α_e. The momentum-sharing distribution of this branching in the collinear limit is described by the QED splitting function $P(z)$. **(b, c)** Processes that contribute to isolated photon subjet production at order $\alpha_e\alpha_s$. Of these, the initial quark term **(b)** dominates.

The probability for a quark to radiate a photon with some angle θ_γ and momentum fraction z_γ is given by:

$$\mathrm{d}P_{q\to q\gamma} = \frac{\alpha_e e^2}{2\pi}\,\frac{\mathrm{d}\theta_\gamma}{\theta_\gamma}\,P(z_\gamma)\,\mathrm{d}z_\gamma, \qquad P(z) = \left(\frac{1+(1-z)^2}{z}\right)_+, \tag{1.2}$$

where $P(z)$ is the (regularized) QED splitting function. Inspired by related work on the $q \to qg$ splitting function in quantum chromodynamics (QCD) [44–49], we use isolated photon subjets to expose the QED $q \to q\gamma$ splitting function $P(z)$. We also investigate the impact of the higher-order α_s corrections in Figs. 1-1b and 1-1c, though we restrict our calculations to the collinear limit.

This work is complementary to earlier experimental investigations of the quark-photon fragmentation function at LEP [7–9, 50]. Notably, Ref. [50] exposed the quark-photon fragmentation function down to $z_\gamma \sim 0.2$ by using cluster shape observables to mitigate meson decay backgrounds. Compared to these studies, the isolated photon subjet approach has the advantage of being perturbatively calculable and likely being easier to implement in the complicated hadronic environment of the LHC. Additionally, the isolated photon subjet condition regulates higher-order terms such as those in Figs. 1-1b and 1-1c, thereby more directly exposing the QED splitting function as opposed to the inclusive photon fragmentation function. Similar to the LEP study, the primary background to isolated photon subjets comes from meson decays, but this can be controlled using a simple angular cut on R_{12}.

The rest of this paper is organized as follows. In Chap. 2, we provide background to common forms of photon isolation. In Chap. 3, we define soft drop isolation, investigate its features, and its analyze its performance in γ-plus-jet events from a parton shower generator. In Chap. 4, we define the isolated photon subjet and compare the extraction of the QED splitting function between a parton shower and an analytic calculation. We conclude with a discussion of future directions in Chap. 5.

Chapter 2

Background

Photon isolation has a long history at colliders and remains an important technique in current use at the LHC. In this chapter, we review the three most common forms of photon isolation: cone isolation, Frixione isolation, and democratic isolation.

2.1 Cone isolation

Cone isolation – in various forms – is by far the most common form of photon isolation currently in use in experiment owing to its simplicity, effectiveness, and longstanding use. While first developed in the LEP era [2–6], cone isolation remains the standard at the LHC [14–18]. However, cone isolation is not used for theoretical calculation because it is not collinear-safe.

In the standard cone procedure, a cone of some radius is drawn around the photon. The photon is declared isolated if it accounts for greater than some large fraction (typically 95%) of the energy in that cone. This may be expressed in terms of the transverse momentum of each particle p_{Ti}, the cone radius R_0, the distance in $y - \phi$ space between the photon and each particle $R_{i,\gamma}$, the photon transverse momentum $p_{T\gamma}$, and the parameter ϵ (usually ~ 0.05) as:

$$\sum_i p_{Ti}\, \Theta\left(R_0 - R_{i\gamma}\right) \leq \epsilon\, p_{T\gamma}. \tag{2.1}$$

It should be noted that different implementations of cone isolation have used variations on Eq. (2.1), typically motivated by the specific backgrounds of the detector. For instance, Refs. [14, 16] use a fixed energy cutoff in place of one that scales with the photon momentum. Refs. [15, 17, 18] use a criterion that scales with the photon momentum plus some offset. However, the basic features of the isolation scheme remain the same.

Because there is no angular requirement other than the R_0 cut, collinear contributions are not completely vetoed. The standard cone is therefore sensitive to the collinear divergences in quark fragmentation. This is not a problem in experiment, where detector granularity naturally regulates the divergence; however, it poses a problem for theoretical calculations. It would in principle be possible to fully eliminate the collinear contributions by taking $\epsilon \to 0$; however, such a technique would restrict the phase space for soft gluon emissions and thus prevent cancellation of the real and virtual infrared divergences. Therefore, although cone isolation is an effective method of mitigating fragmentation backgrounds in experimental prompt photon studies, the fact that it is collinear-unsafe makes it more difficult to compare with calculations using collinear-safe criteria.

2.2 Frixione "smooth" isolation

Frixione or "smooth" isolation [10] has been the preferred photon isolation criterion for perturbative calculations. In contrast to cone isolation, Frixione isolation regulates the collinear divergence by forcing the partonic energy to zero in the collinear limit. In this way, the exact collinear divergence from $q \to q\gamma$ is fully eliminated without in any way restricting the soft phase space, which is required in order to ensure real and virtual cancellation of soft gluon divergences.

Frixione isolation uses an initial angular cut at some radius from the photon R_0. The particles within that radius are then required to pass a momentum cut based on an angular function $X(\Delta R)$, typically called a Frixione function. The full condition may be expressed in terms of the transverse momentum p_{Ti} and distance to the photon

$R_{i,\gamma}$ of each hadronic particle as:[1]

$$\forall\, \Delta R \leq R_0 : \quad \sum_i p_{Ti}\, \Theta\left(\Delta R - R_{i,\gamma}\right) < X(\Delta R). \tag{2.2}$$

There is significant flexibility in the choice of Frixione function $X(\Delta R)$. The most common function used in the literature [10, 11, 17, 18, 51–53] is:

$$X(\Delta R) = p_{T\gamma}\, \epsilon \left(\frac{1-\cos(\Delta R)}{1-\cos(R_0)}\right)^n. \tag{2.3}$$

Under the "tight isolation" parameters outlined in the Les Houches Accords [53], typical parameter values are $\epsilon \sim 0.1$ and $n = 1$.

Frixione isolation fully regulates the collinear divergence of parton-photon fragmentation. It is important to note, however, that this does not mean it fully removes all fragmentation contributions to the isolated photon cross section. Instead, there is a finite, calculable contribution. The parton shower study in Chap. 3.4 demonstrates the presence of low-angle fragmentation. Of course, tightening the isolation requirements can arbitrarily exclude fragmentation; however, one does so at the risk of unduly restricting the soft gluon phase space and thus becoming sensitive to non-perturbative effects. The presence of a finite, calculable fragmentation contribution to isolated photon cross sections is a general feature of all collinear-safe isolation criteria, including soft drop isolation.

2.3 Democratic isolation

In addition to cone and Frixione isolation, there also exists a form of isolation referred to as "democratic isolation" and "the democratic approach." This form of isolation was pioneered in the LEP era for the study of the photon fragmentation function [7–9]. In democratic isolation, the entire event is first clustered into jets, including

[1] Implementations of Frixione isolation often use the transverse energy E_T in place of the transverse momentum p_T. Given the ambiguities in defining transverse energy and the assumption of high energies, we will instead use p_T throughout.

both photons and hadrons. This step, which treats photons and hadrons equally, is the origin of the term "democratic"; undemocratic criteria such as Frixione isolation and cone isolation instead center the isolation scheme around the photon. Following the jet clustering step, a photon is defined to be isolated if it contains greater than some fraction of the energy in its parent jet:

$$\frac{p_{T\gamma}}{p_{T\text{jet}}} > z_{\text{cut}}. \tag{2.4}$$

Because democratic isolation applies the isolation criterion after the event has already been clustered into jets, it is natural for the study of prompt photons within jets. For such parton fragmentation studies, $z_{\text{cut}} = 0.7$ is typical. It is also equally possible to use traditional democratic isolation outside the context of fragmentation for identifying direct photons. One could imagine this being a favorable technique at modern hadronic colliders, where jets are central. However, traditional democratic isolation suffers from the same problem as cone isolation: it contains no angular condition and thus is collinear-unsafe.

While the term "democratic isolation" has typically referred to the particular form of isolation outlined in this section, what makes a criterion democratic is more general. We will use the descriptor "democratic" to refer broadly to isolation criteria which treat hadrons and photons equivalently in the initial clustering. Soft drop isolation, introduced in Chap. 3.1, is one such democratic criterion. However, unlike traditional democratic isolation, soft drop isolation is collinear-safe. We believe that soft drop isolation is the first collinear-safe democratic isolation criterion.

Chapter 3

Photon isolation with soft drop declustering

Soft drop isolation is based on soft drop declustering, a jet grooming algorithm that removes soft and wide-angle radiation to find hard substructure [37]. In this chapter, we show how to tag isolated photons by identifying jets without any substructure. We first define soft drop photon isolation in Chap. 3.1 and show that it is infrared- and collinear-safe. We then show that it is democratic in Chap. 3.2 and compare its behavior to Frixione isolation in Chap. 3.3. In Chap. 3.4, we study soft drop isolation using a parton shower, showing that it performs nearly identically to Frixione isolation.

3.1 Definition of soft drop isolation

The original soft drop procedure begins with a jet of radius R obtained through some clustering algorithm; this paper uses the anti-k_t algorithm [24] with radius $R = 0.4$ throughout. Following this, the jet is reclustered using the Cambridge-Aachen (C/A) algorithm [21–23], yielding an angular-ordered clustering tree. The jet is then declustered into its two C/A parent subjets; if the soft drop condition in Eq. (1.1) is satisfied by the two subjets, then the jet "passes" soft drop and is returned as the soft-dropped jet. Otherwise, the softer (by p_T) of the two subjets is

dropped and the procedure is repeated on the harder of the two subjets.

Soft drop isolation is defined in terms of the soft drop algorithm, but with reversed criteria. If at no point the jet passes the soft drop condition and one is left with a single constituent that cannot be declustered, then the jet "fails" soft drop and the single constituent is returned as the soft-dropped jet.[1] If that single constituent is a photon, then that photon is declared to *pass* soft drop isolation and is labeled as an isolated photon.

Like soft drop, soft drop isolation depends on the parameters z_{cut} and β. For the algorithm to be collinear-safe, we must chose $\beta > 0$. Although there is some flexibility in choosing these parameters, we will for definiteness use the default parameters:

$$z_{\text{cut}} = 0.1, \qquad \beta = 2. \tag{3.1}$$

Given the matching between the soft drop parameter z_{cut} and the Frixione parameter ϵ shown in Chap. 3.3, these parameter choices are roughly equivalent to the standard "tight isolation" parameters outlined in the 2013 Les Houches Accords [53].

We now demonstrate that soft drop isolation is infrared- and collinear-safe when applied to isolated photons; the following logic closely follows Ref. [10].[2] Because soft drop isolation requires the non-photon p_T to vanish as $\Delta R \to 0$, it is intuitive that collinear divergences will be regulated. Collinear divergences in the process $q \to q\gamma$ have amplitude squared proportional to $\frac{1}{\theta}$. For a quark with transverse momentum p_T and a photon with transverse momentum $p_{T\gamma}$, the cross section for an isolated

[1] Strictly speaking, this corresponds to soft drop in "grooming mode" [37]. In "tagging mode", the singlet would simply be vetoed.

[2] As in Ref. [10], this isolation criterion would not be safe for simultaneous soft and collinear divergences. Luckily, this is not relevant for quark and gluon radiation in the presence of a photon, where only one kind of divergence can appear at a time.

photon in the presence of a collinear divergence scales like:

$$\sigma_{\text{SD}} \propto \int \frac{\mathrm{d}\theta}{\theta} \int \mathrm{d}p_T^2 \, \Theta \left[p_{T\gamma} \frac{z_{\text{cut}} \left(\frac{\theta}{R_0} \right)^{\beta}}{1 - z_{\text{cut}} \left(\frac{\theta}{R_0} \right)^{\beta}} - p_T \right], \tag{3.2a}$$

$$\sim p_{T\gamma}^2 \, \frac{(1 - z_{\text{cut}}) \log(1 - z_{\text{cut}}) + z_{\text{cut}}}{\beta(1 - z_{\text{cut}})}, \tag{3.2b}$$

which is clearly convergent. The Heaviside theta function in Eq. (3.2a) is the (inverted) soft drop condition in Eq. (1.1), with the simplifying assumption that $z_{\text{cut}} < \frac{1}{2}$ (which has no effect on the convergence properties).

Crucially, the soft drop condition does not restrict the phase space of soft gluons, since infinitesimal radiation always satisfies Eq. (1.1). Infrared divergences from soft gluons have amplitude squared proportional to $\frac{1}{p_T^2}$. For a gluon with transverse momentum p_T, the cross section for an isolated photon in the presence of an infrared divergence scales like:

$$\sigma_{\text{SD}} \propto \int \mathrm{d}\theta \int^{p_{T\gamma}^2} \frac{\mathrm{d}p_T^2}{p_T^2} \, \Theta \left[p_{T\gamma} \frac{z_{\text{cut}} \left(\frac{\theta}{R_0} \right)^{\beta}}{1 - z_{\text{cut}} \left(\frac{\theta}{R_0} \right)^{\beta}} - p_T \right], \tag{3.3a}$$

$$\sim R_0 \left(\log \left(z_{\text{cut}} \right) - \beta \right), \tag{3.3b}$$

which is again convergent. In Eq. (3.3b), we have used the plus prescription to perform the integral over p_T, which is valid since we have not restricted the phase space of infinitesimally soft gluons and thereby ensured that real-virtual cancellation will occur.

Because soft drop isolation is based on declustering, it is easy to check that infrared- and collinear-safety persists with multiple emissions. Each step in the declustering procedure acts on two subjets, so the way the algorithm handles divergence structures will be the same at each step. In this way, soft drop isolation gives an infrared- and collinear-safe definition for isolated photons.

3.2 Soft drop isolation is democratic

As is clear from the definition in Chap. 3.1, soft drop isolation is a democratic criterion. Much like traditional democratic isolation, soft drop isolation begins by clustering the particles in an event democratically into jets. It is only after the jet has been completely declustered that the soft drop isolation algorithm distinguishes between photons and other particles. Unlike traditional democratic isolation, though, soft drop isolation is collinear-safe. We believe that soft drop isolation is the first democratic collinear-safe photon isolation criterion.

As a democratic criterion, the logic of soft drop isolation is different from that of undemocratic criteria. Instead of testing whether a photon is isolated, soft drop isolation tests whether a jet contains an isolated photon. Democratic isolation techniques are thus more natural for cases where one is testing for multiple isolated photons or for cases where jets are the most natural object. Frixione isolation or cone isolation, on the other hand, are more natural for testing the hardest photon in an event to see if it is isolated.

The fact that soft drop isolation is democratic leads to some mild differences with Frixione isolation. The reasons for this are twofold. First, the fact that the photon is isolated from a jet with radius R means that this isolation radius is not strictly drawn around the photon: the photon might not be exactly at the jet center. Therefore, there can be some differences when the photon is off-center and there are hard features at a distance $\sim R$ from the photon. This has little effect in practice, however, since isolated photons naturally contain most of the momentum of the jet and therefore appear very close to the jet center. Second, soft drop isolation is applied after the event has already been clustered into jet objects, whereas Frixione isolation is applied before the event has been clustered. Frixione isolation thus can allow low-momentum objects at angles $\Delta R < R_0$, whereas such objects are mostly excluded by soft drop isolation (namely, they can only occur due to deviations of the photon from the jet center). These differences between democratic and undemocratic approaches will be explored further in Chap. 3.4.

Soft drop's democratic nature makes it a natural choice for the study of jet structure and substructure. The isolated photon subjet introduced later in Chap. 4.1 is one such example that would be quite unnatural to define with a non-democratic criterion. More broadly, democratic criteria are the natural choice for modern hadron colliders, where jets are ubiquitous objects and clustering techniques like anti-k_t [24] are now used by default.

3.3 Relationship to Frixione isolation

Given the above discussion, it is perhaps surprising that (democratic) soft drop isolation turns out to be equivalent to (undemocratic) Frixione isolation, at least in a particular limit. For small R_0 and small z_{cut}, there are appropriate choices of soft drop parameters such that soft drop isolation and the most common form of Frixione isolation impose the same restriction on two-particle final states. Since this corresponds to the leading order configuration in Fig. 1-1a, we say that the two criteria are equivalent at leading order.

At leading order (corresponding to one additional particle within the photon's isolation cone and taking the small R_0 limit), the Frixione isolation condition in Eq. (2.3) becomes:

$$p_T < p_{T\gamma}\,\epsilon \left(\frac{\Delta R}{R_0}\right)^{2n}. \tag{3.4}$$

It should be noted that this form of $X(\Delta R)$ is equivalent to another Frixione function described in Ref. [10], though this function has not found widespread implementation.

Looking at Eq. (3.2a), the leading-order soft drop criterion with $z_{\text{cut}} < \frac{1}{2}$ is:

$$p_T < p_{T\gamma} \frac{z_{\text{cut}} \left(\frac{\Delta R}{R_0}\right)^{\beta}}{1 - z_{\text{cut}} \left(\frac{\Delta R}{R_0}\right)^{\beta}}. \tag{3.5}$$

This is clearly equivalent to Eq. (3.4) in the small z_{cut} or $\frac{\Delta R}{R_0}$ limits with the identification $z_{\text{cut}} = \epsilon$ and $\beta = 2n$. We should also note that, given the flexibility in choosing a Frixione function, it is possible to choose $X(\Delta R)$ corresponding exactly

to the right-hand side of Eq. (3.5). This form of Frixione isolation would be fully equivalent to soft drop isolation at leading order.[3]

Despite the leading-order equivalence of Frixione and soft drop isolation, there are important differences at higher orders. These differences stem from the fact that soft drop isolation is based on clustering, whereas Frixione isolation is based on a more traditional cone approach. The details of which scheme is stricter depend on the precise phase space configuration, and it is not possible to make a general statement about the differences in multi-particle configurations.

In practice, differences due to higher-order configurations or to differences between Eqs. (2.3) and (3.5) are negligible in most realistic setting, as seen in the parton shower study below. Instead, the primary differences between the two schemes stem from the fact that soft drop isolation is democratic, as already discussed in Chap. 3.2.

3.4 Parton shower study

As a practical test of soft drop isolation, we now perform a parton shower study of isolated photon production in the γ+jet(s) final state. Not surprisingly given their leading order equivalence, we find that soft drop and Frixione isolation perform nearly identically, though soft drop isolation's democratic construction leads to some differences in angular distributions.

We generated events in PYTHIA 8.223 [54, 55] from proton-proton collisions with center-of-mass energy 13 TeV, using the default settings for hadronization and underlying event. We created a sample of 800,000 events from the PYTHIA `PromptPhoton` process, which encodes Compton-like processes that produce a hard photon.[4] Though not shown, we also tested a similar sample of `HardQCD` events, which encodes $2 \to 2$ QCD processes that can produce isolated photons from extra initial-state or final-

[3] This equivalence gives another way to understand why, with appropriate choice in parameters, soft drop isolation is safe to infrared and collinear divergences. Just like Frixione isolation, soft drop isolation fully eliminates collinear fragmentation without restricting the soft gluon phase space.

[4] To ensure that there were sufficient events at high photon p_T, we used binned event generation with bin edges imposed on the hard process of $\hat{p}_T = (100, 200, 300, 400, 600, 800, 1000, 1500, \infty)$ GeV. The events were then reweighted proportional to the generated cross sections.

state emissions; the results did not offer any new qualitative insights compared to the `PromptPhoton` sample. Jet clustering and photon isolation were performed using FastJet 3.2.1 [26]. Soft drop was implemented using the FastJet Contrib 1.026 `RecursiveTools` package [56].

For our event selection, we require an isolated photon with $p_{T\gamma} > 125$ GeV and one hadronic jet with $p_{T\text{jet}} > 100$ GeV. We use the condition $p_{TX} > 25$ GeV to define any additional jets that might appear in the event. A rapidity cut of $|y| < 2$ was applied to the final photon and jet objects after jet clustering. These selection criteria were chosen to roughly match a photon isolation study from ATLAS [18]. For each isolation criterion, we use the tight isolation parameters: $z_{\text{cut}} = \epsilon = 0.1$, $\beta = n/2 = 2$, and $R_0 = 0.4$ [53].

Because of the democratic versus undemocratic distinction, we had to use slightly different photon selection schemes for soft drop and Frixione isolation. For soft drop isolation, we first clustered the event into $R = 0.4$ jets with $p_{TX} > 25$ GeV and tested each jet for an isolated photon with $p_{T\gamma} > 125$ GeV and $|y_\gamma| < 2$; the remaining hadrons from the isolated-photon jet were discarded. For Frixione isolation, every photon with $p_{T\gamma} > 125$ GeV and $|y_\gamma| < 2$ was tested for isolation; if such a photon was found, then the rest of the event was clustered into $R = 0.4$ jets. In the case where an event contained multiple isolated photons, we used only the hardest isolated photon.

In Fig. 3-1a, we show the photon p_T spectrum for each isolation scheme, as well as for the hardest photon (isolated or not) in each event. The soft drop and Frixione distributions are nearly identical, showing that the differences between soft drop and Frixione isolation arising from higher-order effects mentioned in Chap. 3.3 are extremely small in practice. There are on average 5% differences between the isolated photon spectra and the hardest photon spectrum, indicating that both isolation schemes properly identify direct photons. Notably, the two isolated spectra exhibit average differences of less than 0.1% (below the precision of this study), showing that the soft drop isolation and Frixione isolation perform nearly identically.

In Fig. 3-1b, we show the angular distance $R_{\gamma X}$ between the isolated photon and

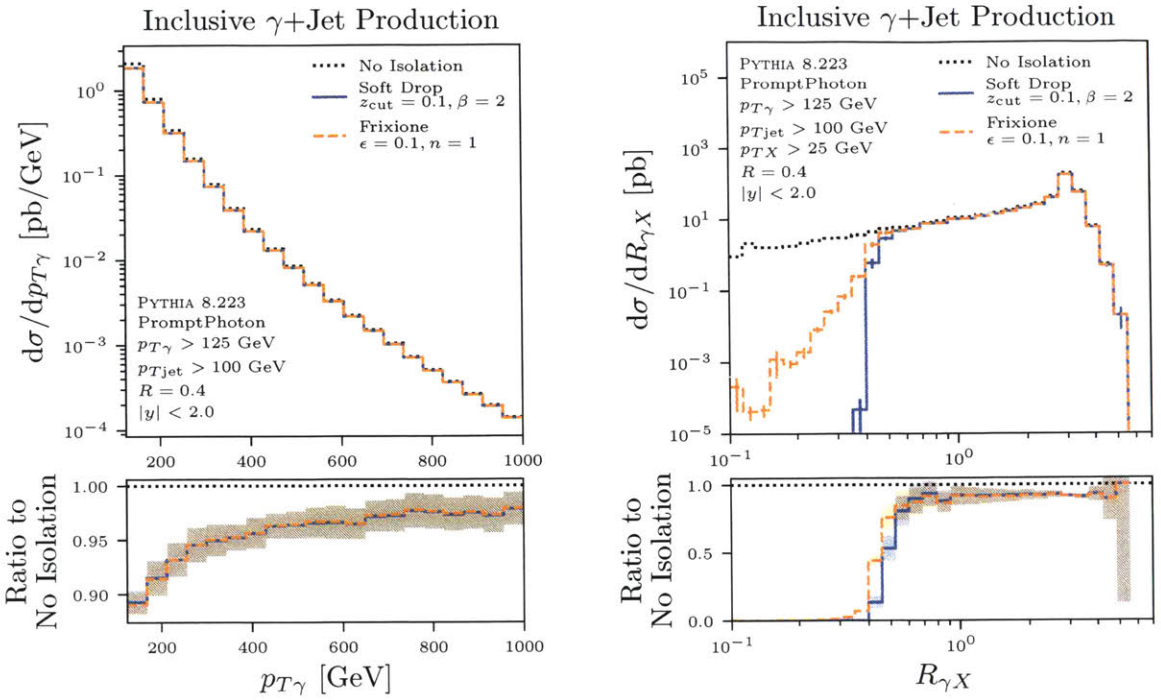

Figure 3-1: Inclusive γ+jet production cross sections from the PYTHIA `PromptPhoton` process, comparing soft drop and Frixione isolation as well as the spectrum of the hardest photon without isolation. **(a)** Photon transverse momentum $p_{T\gamma}$. **(b)** Angle $R_{\gamma X}$ between the photon and the nearest object with $p_{TX} > 25$ GeV, plotted on a logarithmic scale. In both figures, the bottom panels show the ratio of the soft drop and Frixione cross sections to the cross section of the hardest photon in the event without isolation. Shading indicates statistical uncertainty. Although the $p_{T\gamma}$ spectra are nearly identical, there are significant differences in the $R_{\gamma X}$ spectra due to soft drop isolation's democratic nature.

the nearest inclusive jet with $p_{TX} > 25$ GeV and $|y_X| < 2$. As expected, the isolated photon spectra are significantly reduced compared to the non-isolated spectrum for $R_{\gamma X} < 0.4$. The soft drop and Frixione distributions are very similar for $R_{\gamma X} > 0.4$, but there are significant differences between the two isolation schemes in the region $R_{\gamma X} \leq 0.4$. These differences are not due to any differences in strictness but rather to soft drop's democratic construction. Because in Frixione isolation the clustering happens after the isolation step, it is possible for low-energy objects within the photon's isolation cone to become part of one of the inclusive jets X. In contrast, soft drop isolation performs the clustering before the isolation step. Therefore, the only cases in which $R_{\gamma X} < 0.4$ would be permitted are those where the photon is

significantly off-center from the jet axis. These cases are exceedingly rare, and as such, the soft drop isolation spectrum exhibits a relatively hard cutoff at $R_{\gamma X} = 0.4$. We suspect that this hard cutoff behavior will be desirable for future direct photon studies at the LHC.

We used PYTHIA truth information to analyze the performance of each isolation scheme as applied in the above study. Although in the event tagging we used only the hardest isolated photon in the event, the statistics below include all photons that passed the initial p_T and y cuts. Soft drop isolation and Frixione isolation each had 90% efficiency of tagging direct photons as prompt photons. Both isolation criteria achieved 100% rejection of hadronization backgrounds. For final state radiation, which can generate photons both collinear to and well-separated from jets, we analyzed both wide-angle radiation, defined as emissions with angle $\theta > 0.4$, and collinear radiation, defined as emissions with angle $\theta < 0.4$. Both isolation criteria tagged 53% of photons from wide-angle final state radiation as prompt and achieved more than 99% rejection of collinear final state radiation.

The above study validates the use of soft drop isolation to identify direct photons. In the context of PYTHIA, the level of background rejection from both isolation criteria is so high that it was difficult to get a trustable sample of isolated photons from collinear final state radiation or meson decays. Although the above analysis indicates that soft drop isolation and Frixione isolation give very similar indirect photon background rates when using the tight isolation parameters, a detailed study with a detector simulation would be needed to fully quantify the differences.

Chapter 4

Exposing the QED splitting function

Because soft drop isolation is democratic, we can naturally use it in contexts where photons play a key role in the substructure of a jet. The goal of this study is to use the kinematics of isolated photon subjets to expose the QED $q \to q\gamma$ splitting function. We first give a concrete definition of an isolated photon subjet in Chap. 4.1. We then calculate the kinematics of the isolated photon subjet to order α_e in the collinear limit in Chap. 4.2 and show that the photon momentum fraction is directly given by the QED splitting function. We extend this calculation to order $\alpha_e\,\alpha_s$ in Chap. 4.3 and show that the qualitative features do not change. In Chap. 4.4, we test this procedure with a parton shower generator, where we find behavior consistent with the analytic calculations.

4.1 Definition of an isolated photon subjet

Our definition of an isolated photon subjet uses a combination of soft drop declustering and soft drop isolation to identity a quark-like jet with photon substructure. We begin with a jet of radius R obtained through some clustering algorithm (anti-k_T in our study). Soft drop is then applied to the jet with $z_{\text{cut}} = 0.1$, $\beta = 0$, and radius parameter $R_0 = R$, such that soft drop acts like the modified Mass Drop Tagger

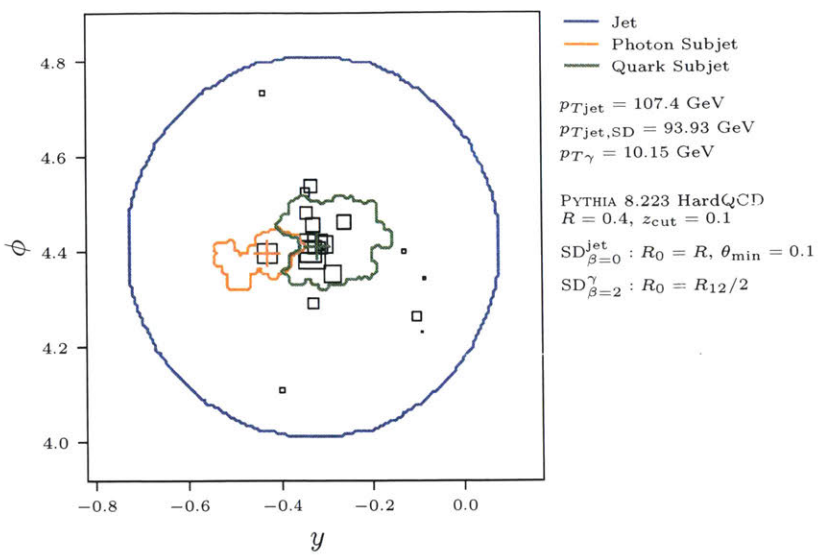

Figure 4-1: Example jet with an isolated photon subjet from a $q \to q\gamma$ splting. For the initial soft drop, denoted $\text{SD}^{\text{jet}}_{\beta=0}$, we used parameters $z_{\text{cut}} = 0.1$, $\beta = 0$, and $R_0 = R = 0.4$. For the subjet isolation criterion, denoted $\text{SD}^{\gamma}_{\beta=2}$, we used parameters $z_{\text{cut}} = 0.1$, $\beta = 2$, and $R_0 = R_{12}/2$, where R_{12} is the angle between the two subjets.

(mMDT) [41]. Events that pass this step now have two prong substructure, and analogous to the QCD splitting function study of Refs. [44, 45], the choice $\beta = 0$ ensures that the z distribution of the resulting subjets is not biased. We then decluster the soft-dropped jet into its two constituent subjets and apply soft drop isolation to each subjet with $z_{\text{cut}} = 0.1$, $\beta = 2$, and radius parameter $R_0 = R_{12}/2$.[1] If exactly one of the subjets passes soft drop isolation, it is labeled as an isolated photon subjet.

In Fig. 4-1, we show an example jet from PYTHIA that contains an isolated photon subjet. The details of the event generation will be given in Chap. 4.4. We see that the first step of soft drop declustering has decreased the active area [57] from the original blue jet to the orange and green subjets. The orange jet consists of only a single photon. The green subjet arises from the fragmentation of a quark parton. Using the PYTHIA event record, we can verify that this configuration does indeed arise from a $q \to q\gamma$ splitting.

The momentum fraction of the isolated photon subjet provides a novel way to ex-

[1] We also performed a study using $R_0 = R$ in the soft drop isolation criterion (while still applying the isolation only to the subjet constituents); although this this version of the criterion does lead to sensible results, we found it to be more sensitive to non-perturbative hadronization effects.

pose the QED splitting function, both in perturbative calculations and in experiment. The QED splitting function, given in Eq. (1.2), describes the probability distribution of the momentum sharing z between the photon and the quark. We define the isolated photon momentum sharing as

$$z_{\text{iso}} = \frac{p_{T\gamma}}{p_{T\text{jet,SD}}}, \tag{4.1}$$

as a proxy for the partonic z, where $p_{T\gamma}$ is the transverse momentum of the isolated photon within the isolated photon subjet and $p_{T\text{jet,SD}}$ is the transverse momentum of the soft-dropped jet. In order to eliminate the primary background from meson decays, we implemented a simple cut on the angle between the two subjets $R_{12} > \theta_{\text{min}}$; a similar cut was used in the CMS study of the QCD splitting function [47]. The details of this cut are discussed further in Chap. 4.4.

4.2 Order α_e calculation

We now calculate the differential cross section in z_{iso} to lowest non-trivial order, focusing on the collinear limit in the fixed-coupling approximation. At order α_e, the cross section is quite simple to evaluate. There is only one term that contributes, corresponding to the single quark-photon branching from Fig. 1-1a. The cross section can be expressed in terms of the initial quark cross section σ_q, the quark charge e_q, the emission angle θ_γ, the momentum sharing z_γ, and the order α_e isolated photon subjet condition $\Theta_{(1,0)}$ as:

$$\frac{\mathrm{d}\sigma_{(1,0)}}{\mathrm{d}z_{\text{iso}}} = \int \mathrm{d}\sigma_q \, \frac{\alpha_e e_q^2}{2\pi} \, \frac{\mathrm{d}\theta_\gamma}{\theta_\gamma} \, \mathrm{d}z_\gamma \, P(z_\gamma) \, \Theta_{(1,0)}, \tag{4.2}$$

where the notation (m, n) refers to the order $\alpha_e^m \alpha_s^n$.

Because at this order the jet consists of only a quark and a photon, the procedure in Chap. 4.1 always identifies a quark subjet and a photon subjet, which is automatically an isolated subjet. The only conditions are that the two particles fall within the jet radius, that the jet as a whole pass the initial soft drop condition, and that the two

subjets pass the minimum relative-angle condition:

$$\Theta_{(1,0)} = \Theta\left[z_\gamma - z_{\text{cut}}\right]\Theta\left[(1-z_\gamma) - z_{\text{cut}}\right]\delta\left[z_{\text{iso}} - z_\gamma\right]\Theta\left[R - \theta_\gamma\right]\Theta\left[\theta_\gamma - \theta_{\min}\right]. \quad (4.3)$$

Inserting this into Eq. (4.2), our cross section neatly factorizes into angular and momentum-fraction components, yielding a z_{iso} distribution that is directly proportional to the splitting function:

$$\begin{aligned}\frac{\mathrm{d}\sigma_{(1,0)}}{\mathrm{d}z_{\text{iso}}} &= \sigma_q \frac{\alpha_e e_q^2}{2\pi}\int_{\theta_{\min}}^{R}\frac{\mathrm{d}\theta_\gamma}{\theta_\gamma}\int_{z_{\text{cut}}}^{1-z_{\text{cut}}}\mathrm{d}z_\gamma\, P(z_\gamma)\,\delta\left[z_{\text{iso}} - z_\gamma\right] \\ &= \sigma_q \frac{\alpha_e e_q^2}{2\pi}\log\left(\frac{R}{\theta_{\min}}\right) P(z_{\text{iso}})\,\Theta\left[z_{\text{iso}} - z_{\text{cut}}\right]\,\Theta\left[1 - z_{\text{cut}} - z_{\text{iso}}\right]\end{aligned} \quad (4.4)$$

Thus, at order α_e the isolated photon subjet observable directly exposes the QED $q \to q\gamma$ splitting function.

The initial quark cross section σ_q is the cross section for quark jet production at the p_T scale of the calculation. At order α_e, σ_q appears only as a factor in normalization; at order $\alpha_e\alpha_s$, where both quark jet and gluon jet terms contribute, the ratio of σ_q to its gluon jet production counterpart σ_g is relevant. These values are discussed in detail in Chap. 4.3.

4.3 Order $\alpha_e\alpha_s$ calculation

Going to higher orders, one might worry that the simple behavior in Eq. (4.4) would be spoiled by QCD radiation within the jet. This turns out not to be the case. The reason is that the isolated photon subjet condition regulates singularities collinear to the photon, such that higher-order terms in the inclusive parton-photon fragmentation function are controlled without diminishing the order α_e splitting function. Although there are still higher-order corrections, they are significantly reduced compared to the raw fragmentation function. In this way, the isolated photon subjet more directly exposes the QED splitting function instead of merely exposing the parton-photon fragmentation function.

We can verify the above statements by performing a calculation of the z_{iso} distribution at order $\alpha_e\,\alpha_s$. At this order, analytic calculations of the cross section become considerably more involved, even restricting to the collinear limit with fixed coupling and strongly-ordered emissions. Two terms contribute to the cross section: the case in which an initial quark emits a photon and a gluon (Fig. 1-1b), and the case in which an initial gluon splits into a quark-antiquark pair, one of which then radiates a photon (Fig. 1-1c). Of these two terms, the initial-quark case is dominant, as the initial gluon will be almost entirely excluded by the subjet isolation step.

We work in the strongly-ordered limit, with the emission ordering determined by a generalized virtuality $Q = z(1-z)\theta^n$. By changing the value of n, we can get a sense of the uncertainties in our calculation, though we emphasize that we have not performed a comprehensive uncertainty estimate. The choice $n = 1$ corresponds to k_t ordering, $n = 2$ corresponds to a mass ordering, and we also test $n = 1/2$ for completeness. For the initial-quark diagram in Fig. 1-1b, the ordering determines whether the gluon or the photon is emitted first. For the initial-gluon diagram in Fig. 1-1c, the gluon-to-quarks splitting is required to occur first.

The total differential cross section in the observable z_{iso} can be expressed in terms of the initial-quark cross section σ_q, the initial-gluon cross section σ_g, each emission's angle θ and momentum sharing z, the azimuthal angle with respect to the jet axis between emissions ϕ, the $q \to q\gamma$ and $q \to qg$ splitting function P, the $g \to q\bar{q}$ splitting function P_{qg}, and the order $\alpha_e\alpha_s$ isolated photon subjet condition $\Theta_{(1,1)}$:[2]

$$\begin{aligned}\frac{\mathrm{d}\sigma_{(1,1)}}{\mathrm{d}z_{\text{iso}}} = &\int \mathrm{d}\sigma_q \, \frac{\alpha_e e_q^2}{2\pi}\frac{\mathrm{d}\theta_\gamma}{\theta_\gamma}\,\mathrm{d}z_\gamma\, P(z_\gamma)\,\frac{\alpha_s C_F}{2\pi}\frac{\mathrm{d}\theta_g}{\theta_g}\,\mathrm{d}z_g\, P(z_g)\,\frac{\mathrm{d}\phi}{2\pi}\,\Theta_{(1,1)}\left[p_q, p_g, p_\gamma\right] \\ &+ 2\int \mathrm{d}\sigma_g \, \frac{\alpha_s T_F}{2\pi}\frac{\mathrm{d}\theta_q}{\theta_q}\,\mathrm{d}z_q\, P_{qg}(z_q)\,\frac{\alpha_e e_q^2}{2\pi}\frac{\mathrm{d}\theta_\gamma}{\theta_\gamma}\,\mathrm{d}z_\gamma\, P(z_\gamma)\,\frac{\mathrm{d}\phi}{2\pi}\,\Theta_{(1,1)}\left[p_q, p_{\bar{q}}, p_\gamma\right].\end{aligned} \tag{4.5}$$

For simplicity of presentation, we do not give the precise functional form for $\Theta_{(1,1)}$. This function contains the clustering, initial soft drop, and subjet isolation steps

[2]The name z_g for the momentum fraction of the gluon should not be confused with the groomed momentum fraction from Ref. [44].

and depends on the four-momenta of the final-state particles. These four-momenta in turn depend on how the branching variables z and θ are mapped to physical kinematics. We decide to define four-momenta by conserving energy and momentum transverse to the branching axis (i.e. k_t) at each branching.[3] Because the ordering of emissions changes how energy and momentum are conserved, the virtuality ordering is implicitly contained in the expressions for the four-momenta. While it is possible to express $\Theta_{(1,1)}$ in terms of the splitting kinematics (and we have), it is tedious and unenlightening.

In practice, we use Monte Carlo integration to perform the integral in Eq. (4.5). We generate "events" with each parameter z and θ selected according to a uniform distribution with a lower bound of 0.001, and ϕ distributed uniformly in $[0, 2\pi)$. Each event is assigned a weight equal to the integrand in Eq. (4.5). To implement the plus prescription on z_g in the initial quark case, for each event with an initial quark, we generated a second event with the same values of $\{z_\gamma, \theta_\gamma, \theta_g\}$, a negative weight, and z_g selected according to a uniform distribution over $[0, 0.001)$. We use the splitting kinematics to construct three massless four-vectors, after which we use the same FastJet tools as in Chap. 3.4 to implement the isolated photon subjet procedure.

Although the kinematics of Eq. (4.5) are independent of the jet momentum scale, the parameters σ_q, σ_g, and α_s all depend on the momentum. We performed our analysis at jet transverse momenta of $p_T = \{100, 200, 400, 800\}$ GeV. The initial quark jet cross section σ_q and the gluon jet cross section σ_g were determined for each momentum in Pythia. At 400 GeV, we obtained $\sigma_q/\sigma_g = 0.63$. Throughout we assume flavor universality, such that the z_{iso} distribution does not depend on the quark charges except as a normalization. At each energy we used a fixed-coupling approximation for the value of α_s, evaluated at $\mu = p_T R$:

$$\alpha_s(\mu^2) = \frac{\alpha_s(m_Z^2)}{1 + \alpha_s(m_Z^2)\, b_0 \log\left(\frac{\mu^2}{m_Z^2}\right)}, \tag{4.6}$$

[3] We do not conserve longitudinal momentum in this process, which is consistent in the collinear limit.

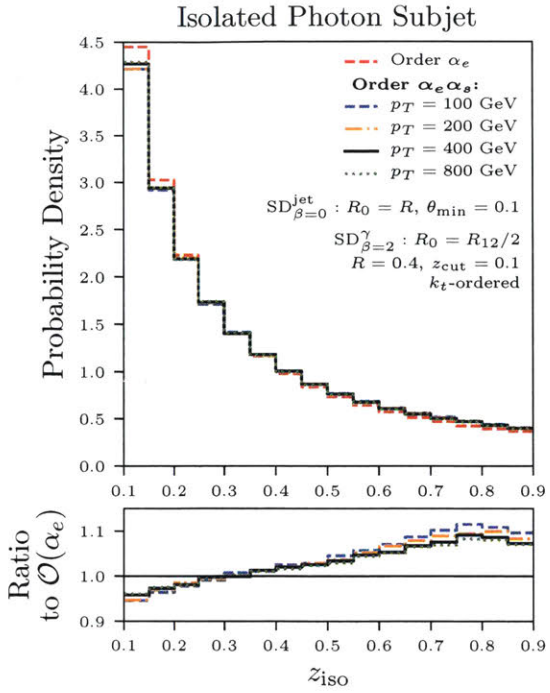

Figure 4-2: Probability densities for isolated photon subjet momentum fraction z_{iso} at order α_e and order $\alpha_e\alpha_s$ in the collinear limit. Shown are results at $p_T = \{100, 200, 400, 800\}$ GeV.

where $b_0 = (33 - 2N_f)/(12\pi)$. Here N_f is defined as the number of flavors available at the scale μ.

In Fig. 4-2, we show the order $\alpha_e\alpha_s$ probability densities in z_{iso}. Compared to the order α_e cross section, the $\alpha_e\alpha_s$ terms yield at most a 10% suppresion, and as such, the z_{iso} distribution largely resembles the basic quark-photon splitting function. The order $\alpha_e\alpha_s$ initial gluon term is suppressed at a factor of ~ 0.1 compared to the order $\alpha_e\alpha_s$ initial quark term, so it only contributes a correction to the order α_e result at a factor of ~ 0.01. Changing the virtuality scale n has around a 2% effect between $n = 1/2$ and $n = 2$, so we expect that neglected higher-order contributions to the cross section will have a modest impact on the final shape of the distribution.

4.4 Parton shower study

We now perform a parton shower study in PYTHIA 8.223, with the aim of testing the robustness of the z_{iso} distribution to hadronization effects. We generate events from

the HARDQCD process, which encodes $2 \to 2$ hard QCD events. We made event samples for $p_{T\text{min}} = \{100, 200, 400, 800\}$ GeV, each with 20 million events.[4] Because the efficiency for finding isolated photon subjets is so small, we turn off initial state radiation and underlying event to speed up event generation, leaving all other PYTHIA settings at their default values. Since the isolated photon subjet condition is based on jet grooming, we do not expect these modifications to make a large impact on our results, though a detailed study of these effects is warranted.

Events were clustered into anti-k_T jets of radius $R = 0.4$ with a transverse momentum cut $p_{T\text{jet}} > p_{T\text{min}}$ and a rapidity cut $|y_{\text{jet}}| < 2$. The clustering step and the isolated photon subjet step were implemented using FASTJET and FASTJET CONTRIB using the same code for the order $\alpha_e\,\alpha_s$ calculation in Chap. 4.3.

At low energies and low angles, the isolated photon subjet sample was found to be dominated by neutral pion decays: because the observable identifies the photon "prongs" of a jet, it was in many cases identifying one of the photons produced in such a decay. These contributions are relatively easily avoided by choosing appropriate values for θ_{min} and $p_{T\text{min}}$; whereas pion decays become more collinear at higher energies, the angular aspect of QED branchings is energy-independent. Using PYTHIA truth information, we were able to identify signal (photons from QED branchings) and background (all other photons). In Fig. 4-3a, we show signal and background rates for isolated photons at different values of θ_{min} and $p_{T\text{min}}$. We choose to use $p_{T\text{min}} = 400$ GeV and $\theta_{\text{min}} = 0.1$ for the remainder of this study, as these values yielded signal cross section of around 3 pb for a background cross section of around 0.006 pb. This value of θ_{min} is also a sensible cut from the perspective of the granularity of a typical hadronic calorimeter. This corresponds to around 150,000 recorded events for the 45 fb^{-1} 2017 run of CMS, of which only about 300 events would be from the pion background [58].

In Fig. 4-3b, we show the probability distribution in z_{iso} for $p_{T\text{min}} = 400$ GeV and $\theta_{\text{min}} = 0.1$ plotted against the corresponding distributions for order α_e and $\alpha_e\,\alpha_s$ theoretical results. The PYTHIA distribution exhibits quite good correspondence with the

[4] In each case, we set the PYTHIA parameter $\hat{p}_{T\text{min}}$ to be 20% lower than the jet cut.

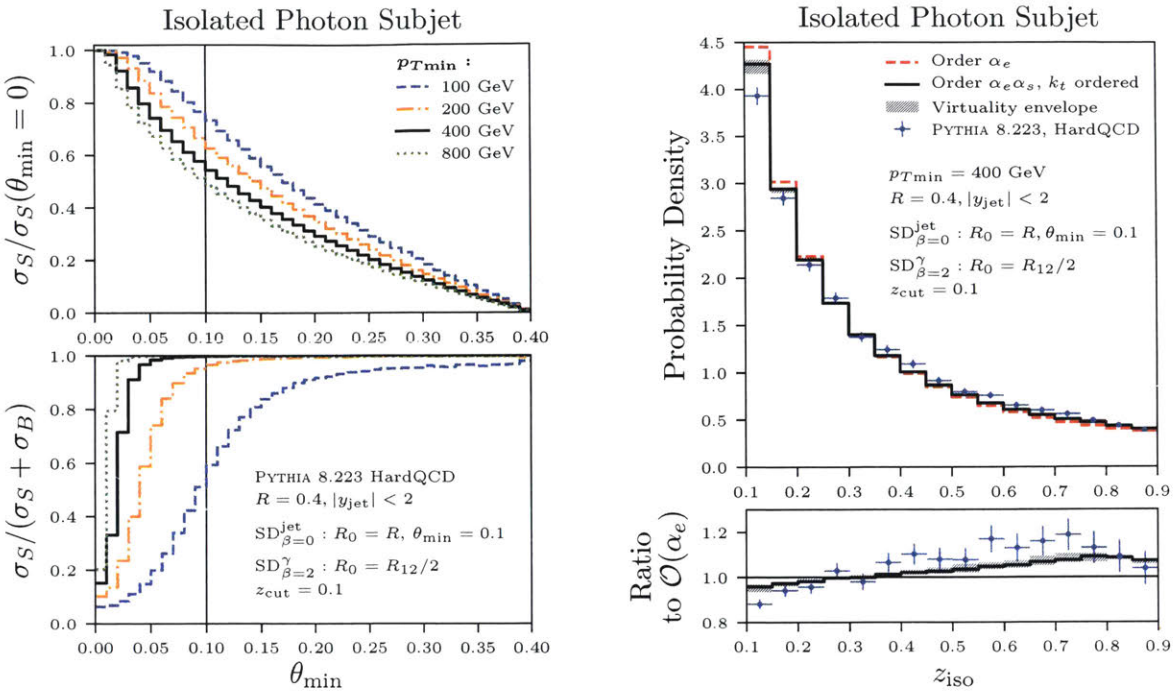

(a) (b)

Figure 4-3: **(a)** Top: PYTHIA cross sections of the $q \to q\gamma$ signal as a function of $\theta_{\min}$, given as a ratio to the cross section at $\theta_{\min} = 0$. Signal also decreases with p_T, and we found $\sigma_S(\theta_{\min} = 0) = \{1000, 96, 6.2, 0.22\}$ pb at $p_{T\min} = \{100, 200, 400, 800\}$ GeV. Bottom: ratio of signal cross section to the sum of signal and background cross sections. For our case study analysis we used $p_{T\min} = 400$ GeV and $\theta_{\min} = 0.1$. **(b)** Probability distributions in z_{iso} for the isolated photon subjet at order α_e, order $\alpha_e\alpha_s$, and in PYTHIA with $p_{T\min} = 400$ GeV.

perturbative results. It appears that the higher-order corrections are somewhat amplified, albeit with the same functional form. This is likely due to non-perturbative effects arising from the non-collinear hadronization of the quark subjet, which introduces some soft radiation into the photon subjet. In order to test the effect of hadronization, we applied the same isolated photon subjet criterion to PYTHIA events with hadronization disabled and found slightly closer matching to the $\mathcal{O}(\alpha_e\alpha_s)$ result.

It is clear from Fig. 4-3b that, even with higher order effects, the isolated photon subjet clearly exposes the form of the QED splitting function. This parton shower study therefore validates the use of isolated photon subjets to expose the splitting function in realistic collider scenarios.

Chapter 5

Conclusion

In this first half of this paper, we introduced soft drop isolation, a new form of photon isolation based on techniques from jet substructure. Soft drop isolation is infrared- and collinear-safe, democratic, and equivalent at leading order to the most common form of Frixione isolation, making it well-suited to identify direct photons at the LHC. In the second half of this paper, we turned to indirect photons, using a combination of soft drop declustering and soft drop isolation to define isolated photon subjets. We showed how the momentum fraction carried by isolated photon subjets can be used to expose the QED splitting function, which describes the momentum sharing distribution of quark-photon branchings in the collinear limit.

As a further extension of this method, soft drop isolation could provide new way to handle detector granularity. All collinear-safe isolation criteria are complicated by granularity, which forces the isolation to cut off at the detector's angular resolution when implemented in experiment. This makes matching between calculations (in which there is no cut-off) and experimental implementations more difficult. Ref. [51] has addresses this issue for Frixione isolation by using a set of cocentric cones instead of a smoothly varying cone. Treating angular resolution with soft drop isolation would be quite straightforward, owing to its clustering basis. One could introduce a parameter θ_{min} equal to the detector's angular resolution (analogous to that in Chap. 4) and stop the declustering when the angle between the two subjets was less than θ_{min}. Because the Cambridge-Achen declustering is angular-ordered, this means

that the isolation would only treat features with angular separation greater than the detector resolution. While this is not identical to the behavior in granular detectors, we expect it to very closely approximate that behavior.

It is possible to envision a number of extensions to the QED splitting analysis performed in Chap. 4. Parallel to the analysis performed in Ref. [59] for the QCD splitting function, the isolated photon subjet criterion could be used in combination with flavor-tagging to identify heavy-flavor QED splittings. Additionally, the same QED splitting analysis could be performed on leptons. While lepton QED splittings are well studied given the lack of lepton hadronization, it could nevertheless be an interesting test of this new democratic isolation scheme.

Finally, the isolated photon subjet also opens the door to a broad spectrum of photon substructure studies and observables beyond the QED splitting function. Isolated photon subjets could be used to study substructure within photon jets [60]: jets composed primarily of photons that arise from scenarios beyond the standard model. This work would very naturally complement and build on Ref. [60], which uses a variety of substructure observables to study the properties of photon jets. Whereas the isolated photon subjet study in this paper analyzed two-prong substructure with one photon subjet, future areas of interest include cases with two isolated photon subjets. Additionally, isolated photon subjets could be used to tag boosted decays such as $h \to Z\gamma$ or, more broadly, possible decays to jets and photons of boosted beyond-the-standard-model objects.

Isolated photon subjets provide a powerful framework for the study of QED substructure within QCD jets. We hope that the existence of this technique – and more generally, of a democratic, collinear-safe photon isolation criterion – will encourage the further development of photon-based jet substructure observables.

Bibliography

[1] Z. Hall and J. Thaler, *Photon Isolation and Jet Substructure*, MIT-CTP/5011, 2018.

[2] H. Baer, J. Ohnemus, and J. F. Owens, *A Next-to-leading Logarithm Calculation of Direct Photon Production*, *Phys. Rev.* **D42** (1990) 61–71.

[3] E. L. Berger and J.-w. Qiu, *Calculations of prompt photon production in QCD*, *Phys. Rev.* **D44** (1991) 2002–2024.

[4] G. Kramer and B. Lampe, *QCD corrections to final state photon Bremsstrahlung in e- e- annihilation*, *Phys. Lett.* **B269** (1991) 401–406.

[5] Z. Kunszt and Z. Trocsanyi, *QCD corrections to photon production in association with hadrons in e+ e- annihilation*, *Nucl. Phys.* **B394** (1993) 139–168, [hep-ph/9207232].

[6] E. W. N. Glover and W. J. Stirling, *Isolated hard photon radiation in multi - jet production at LEP*, *Phys. Lett.* **B295** (1992) 128–135.

[7] **ALEPH** Collaboration, D. Buskulic et al., *First measurement of the quark to photon fragmentation function*, *Z. Phys.* **C69** (1996) 365–378.

[8] E. W. N. Glover and A. G. Morgan, *Measuring the photon fragmentation function at LEP*, *Z. Phys.* **C62** (1994) 311–322.

[9] A. Gehrmann-De Ridder, T. Gehrmann, and E. W. N. Glover, *Radiative corrections to the photon + 1 jet rate at LEP*, *Phys. Lett.* **B414** (1997) 354–361, [hep-ph/9705305].

[10] S. Frixione, *Isolated photons in perturbative QCD*, *Phys. Lett.* **B429** (1998) 369–374, [hep-ph/9801442].

[11] L. Cieri, *Diphoton isolation studies*, *Nucl. Part. Phys. Proc.* **273-275** (2016) 2033–2039, [arXiv:1510.0687].

[12] **ALEPH** Collaboration, D. Buskulic et al., *Measurement of prompt photon production in hadronic Z decays*, *Z. Phys.* **C57** (1993) 17–36.

[13] E. W. N. Glover and A. G. Morgan, *The Photon + 1 jet event rate with the cone algorithm in hadronic events at LEP*, *Phys. Lett.* **B334** (1994) 208–214.

[14] **CMS** Collaboration, V. Khachatryan et al., *Measurement of the Isolated Prompt Photon Production Cross Section in pp Collisions at $\sqrt{s} = 7$ TeV*, *Phys. Rev. Lett.* **106** (2011) 082001, [arXiv:1012.0799].

[15] **CMS** Collaboration, S. Chatrchyan et al., *Measurement of the Differential Cross Section for Isolated Prompt Photon Production in pp Collisions at 7 TeV*, *Phys. Rev.* **D84** (2011) 052011, [arXiv:1108.2044].

[16] **ATLAS** Collaboration, G. Aad et al., *Measurement of the inclusive isolated prompt photon cross section in pp collisions at $\sqrt{s} = 7$ TeV with the ATLAS detector*, *Phys. Rev.* **D83** (2011) 052005, [arXiv:1012.4389].

[17] **ATLAS** Collaboration, M. Aaboud et al., *Measurement of the production cross section of three isolated photons in pp collisions at $\sqrt{s} = 8$ TeV using the ATLAS detector*, *Phys. Lett.* **B781** (2018) 55–76, [arXiv:1712.0729].

[18] **ATLAS** Collaboration, M. Aaboud et al., *Measurement of the cross section for isolated-photon plus jet production in pp collisions at $\sqrt{s} = 13$ TeV using the ATLAS detector*, *Phys. Lett.* **B780** (2018) 578–602, [arXiv:1801.0011].

[19] S. Catani, Y. L. Dokshitzer, M. H. Seymour, and B. R. Webber, *Longitudinally invariant K_t clustering algorithms for hadron hadron collisions*, *Nucl. Phys.* **B406** (1993) 187–224.

[20] S. D. Ellis and D. E. Soper, *Successive combination jet algorithm for hadron collisions*, *Phys. Rev.* **D48** (1993) 3160–3166, [hep-ph/9305266].

[21] Y. L. Dokshitzer, G. D. Leder, S. Moretti, and B. R. Webber, *Better jet clustering algorithms*, *JHEP* **08** (1997) 001, [hep-ph/9707323].

[22] M. Wobisch and T. Wengler, *Hadronization corrections to jet cross-sections in deep inelastic scattering*, in *Monte Carlo generators for HERA physics. Proceedings, Workshop, Hamburg, Germany, 1998-1999*, pp. 270–279, 1998. hep-ph/9907280.

[23] M. Wobisch, *Measurement and QCD analysis of jet cross-sections in deep inelastic positron proton collisions at $\sqrt{s} = 300$ GeV*. PhD thesis, Aachen, Tech. Hochsch., 2000.

[24] M. Cacciari, G. P. Salam, and G. Soyez, *The Anti-k(t) jet clustering algorithm*, *JHEP* **04** (2008) 063, [arXiv:0802.1189].

[25] G. P. Salam, *Towards Jetography*, *Eur. Phys. J.* **C67** (2010) 637–686, [arXiv:0906.1833].

[26] M. Cacciari, G. P. Salam, and G. Soyez, *FastJet User Manual*, *Eur. Phys. J.* **C72** (2012) 1896, [arXiv:1111.6097].

[27] M. H. Seymour, *Tagging a heavy Higgs boson*, in *ECFA Large Hadron Collider Workshop, Aachen, Germany, 4-9 Oct 1990: Proceedings.2.*, pp. 557–569, 1991.

[28] M. H. Seymour, *Searches for new particles using cone and cluster jet algorithms: A Comparative study*, *Z. Phys.* **C62** (1994) 127–138.

[29] J. M. Butterworth, B. E. Cox, and J. R. Forshaw, *WW scattering at the CERN LHC*, *Phys. Rev.* **D65** (2002) 096014, [hep-ph/0201098].

[30] J. M. Butterworth, J. R. Ellis, and A. R. Raklev, *Reconstructing sparticle mass spectra using hadronic decays*, *JHEP* **05** (2007) 033, [hep-ph/0702150].

[31] J. M. Butterworth, A. R. Davison, M. Rubin, and G. P. Salam, *Jet substructure as a new Higgs search channel at the LHC*, *Phys. Rev. Lett.* **100** (2008) 242001, [arXiv:0802.2470].

[32] A. Abdesselam et al., *Boosted objects: A Probe of beyond the Standard Model physics*, *Eur. Phys. J.* **C71** (2011) 1661, [arXiv:1012.5412].

[33] A. Altheimer et al., *Jet Substructure at the Tevatron and LHC: New results, new tools, new benchmarks*, *J. Phys.* **G39** (2012) 063001, [arXiv:1201.0008].

[34] A. Altheimer et al., *Boosted objects and jet substructure at the LHC. Report of BOOST2012, held at IFIC Valencia, 23rd-27th of July 2012*, *Eur. Phys. J.* **C74** (2014), no. 3 2792, [arXiv:1311.2708].

[35] D. Adams et al., *Towards an Understanding of the Correlations in Jet Substructure*, *Eur. Phys. J.* **C75** (2015), no. 9 409, [arXiv:1504.0067].

[36] A. J. Larkoski, I. Moult, and B. Nachman, *Jet Substructure at the Large Hadron Collider: A Review of Recent Advances in Theory and Machine Learning*, arXiv:1709.0446.

[37] A. J. Larkoski, S. Marzani, G. Soyez, and J. Thaler, *Soft Drop*, *JHEP* **05** (2014) 146, [arXiv:1402.2657].

[38] S. D. Ellis, C. K. Vermilion, and J. R. Walsh, *Techniques for improved heavy particle searches with jet substructure*, *Phys. Rev.* **D80** (2009) 051501, [arXiv:0903.5081].

[39] S. D. Ellis, C. K. Vermilion, and J. R. Walsh, *Recombination Algorithms and Jet Substructure: Pruning as a Tool for Heavy Particle Searches*, *Phys. Rev.* **D81** (2010) 094023, [arXiv:0912.0033].

[40] D. Krohn, J. Thaler, and L.-T. Wang, *Jet Trimming*, *JHEP* **02** (2010) 084, [arXiv:0912.1342].

[41] M. Dasgupta, A. Fregoso, S. Marzani, and G. P. Salam, *Towards an understanding of jet substructure*, *JHEP* **09** (2013) 029, [arXiv:1307.0007].

[42] **CMS** Collaboration, A. M. Sirunyan et al., *Particle-flow reconstruction and global event description with the CMS detector*, *JINST* **12** (2017), no. 10 P10003, [arXiv:1706.0496].

[43] **ATLAS** Collaboration, M. Aaboud et al., *Jet reconstruction and performance using particle flow with the ATLAS Detector*, *Eur. Phys. J.* **C77** (2017), no. 7 466, [arXiv:1703.1048].

[44] A. J. Larkoski, S. Marzani, and J. Thaler, *Sudakov Safety in Perturbative QCD*, *Phys. Rev.* **D91** (2015), no. 11 111501, [arXiv:1502.0171].

[45] A. Larkoski, S. Marzani, J. Thaler, A. Tripathee, and W. Xue, *Exposing the QCD Splitting Function with CMS Open Data*, *Phys. Rev. Lett.* **119** (2017), no. 13 132003, [arXiv:1704.0506].

[46] A. Tripathee, W. Xue, A. Larkoski, S. Marzani, and J. Thaler, *Jet Substructure Studies with CMS Open Data*, *Phys. Rev.* **D96** (2017), no. 7 074003, [arXiv:1704.0584].

[47] **CMS** Collaboration, A. M. Sirunyan et al., *Measurement of the Splitting Function in pp and Pb-Pb Collisions at* $\sqrt{s_{\mathrm{NN}}} = 5.02$ *TeV*, *Phys. Rev. Lett.* **120** (2018), no. 14 142302, [arXiv:1708.0942].

[48] **ALICE** Collaboration, D. Caffarri, *Exploring jet substructure with jet shapes in ALICE*, *Nucl. Phys.* **A967** (2017) 528–531, [arXiv:1704.0523].

[49] **STAR** Collaboration, K. Kauder, *Measurement of the Shared Momentum Fraction* z_g *using Jet Reconstruction in p+p and Au+Au Collisions with STAR*, *Nucl. Phys.* **A967** (2017) 516–519, [arXiv:1704.0304].

[50] **OPAL** Collaboration, K. Ackerstaff et al., *Measurement of the quark to photon fragmentation function through the inclusive production of prompt photons in hadronic Z0 decays*, *Eur. Phys. J.* **C2** (1998) 39–48, [hep-ex/9708020].

[51] **SM and NLO Multileg Working Group** Collaboration, T. Binoth et al., *The SM and NLO Multileg Working Group: Summary report*, in *Physics at TeV colliders. Proceedings, 6th Workshop, dedicated to Thomas Binoth, Les Houches, France, June 8-26, 2009*, pp. 21–189, 2010. arXiv:1003.1241.

[52] **SM MC Working Group, SM and NLO MULTILEG Working Group** Collaboration, J. Alcaraz Maestre et al., *The SM and NLO Multileg and SM MC Working Groups: Summary Report*, in *Proceedings, 7th Les Houches Workshop on Physics at TeV Colliders: Les Houches, France, May 30-June 17, 2011*, pp. 1–220, 2012. arXiv:1203.6803.

[53] J. R. Andersen et al., *Les Houches 2013: Physics at TeV Colliders: Standard Model Working Group Report*, arXiv:1405.1067.

[54] T. Sjostrand, S. Mrenna, and P. Z. Skands, *PYTHIA 6.4 Physics and Manual*, *JHEP* **05** (2006) 026, [hep-ph/0603175].

[55] T. Sjstrand, S. Ask, J. R. Christiansen, R. Corke, N. Desai, P. Ilten, S. Mrenna, S. Prestel, C. O. Rasmussen, and P. Z. Skands, *An Introduction to PYTHIA 8.2*, *Comput. Phys. Commun.* **191** (2015) 159–177, [arXiv:1410.3012].

[56] "FastJet Contrib 1.026." http://fastjet.hepforge.org/contrib/.

[57] M. Cacciari, G. P. Salam, and G. Soyez, *The Catchment Area of Jets*, *JHEP* **04** (2008) 005, [arXiv:0802.1188].

[58] "CMS Luminosity – Public Results." https://twiki.cern.ch/twiki/bin/view/CMSPublic/LumiPublicResults#2017_proton_proton_13_TeV_collis. Accessed: 2018-05-09.

[59] P. Ilten, N. L. Rodd, J. Thaler, and M. Williams, *Disentangling Heavy Flavor at Colliders*, *Phys. Rev.* **D96** (2017), no. 5 054019, [arXiv:1702.0294].

[60] S. D. Ellis, T. S. Roy, and J. Scholtz, *Phenomenology of Photon-Jets*, *Phys. Rev.* **D87** (2013), no. 1 014015, [arXiv:1210.3657].